ELSEVIER

Journal of Biomechanics 41 (2008) 2047–2054

JOURNAL OF BIOMECHANICS

www.elsevier.com/locate/jbiomech
www.JBiomech.com

Computational model of airflow in upper 17 generations of human respiratory tract

T. Gemci[a,*], V. Ponyavin[c], Y. Chen[a,b], H. Chen[b], R. Collins[a,b]

[a]*Biomedical Engineering Program, University of Nevada, Las Vegas, 4505 Maryland Parkway, Box 454027, NV 89154, USA*
[b]*Mechanical Engineering Department, University of Nevada, 4505 Maryland Parkway, Box 454027, Las Vegas, NV 89154, USA*
[c]*General Electric Company, Accessory Systems Engineering, Greenville, SC, USA*

Accepted 20 December 2007

Abstract

Computational fluid dynamics (CFD) studies of airflow in a digital reference model of the 17-generation airway (bronchial tree) were accomplished using the FLUENT® computational code, based on the anatomical model by Schmidt et al. [2004. A digital reference model of the human bronchial tree. Computerized Medical Imaging and Graphics 28, 203–211]. The lung model consists of 6.744×10^6 unstructured tetrahedral computational cells. A steady-state airflow rate of 28.3 L/min was used to simulate the transient turbulent flow regime using a large eddy simulation (LES) turbulence model. This CFD mesh represents the anatomically realistic asymmetrical branching pattern of the larger airways. It is demonstrated that the nature of the secondary vortical flows, which develop in such asymmetric airways, varies with the specific anatomical characteristics of the branching conduits.

Keywords: Tracheobronchial airways; Human tracheobronchial airway model; Asymmetric bronchial tree; Computational; LES model

1. Introduction

A widely used model for CFD simulations and predictions of gas transport, particle deposition and dosimetry in the human lung is that characterized by a regular, dichotomous branching pattern (Snyder et al., 1981; Zhao and Lieber, 1994; Calay et al., 2002; Lee and Lee, 2002; Liu et al., 2003; Kleinstreuer and Zhang, 2003; Nowak et al., 2003; Shi et al., 2004; Zhang and Kleinstreuer, 2004). Nowak et al., (2003) and Cebral and Summer (2004) used computed tomography (CT) scans to characterize the tracheobronchial airways more realistically, albeit only down to the fourth generation subunit (G0–G4). Kriete et al. (2004) reported the oxygen gas transport and particle deposition in a digital reference model based on data by Schmidt et al. (2004) with a limited 29-terminal bronchi outlet; whereas, our study includes all 720 bronchi outlets. The final mesh of Kriete et al. (2004) contained a total of 456,463 prism and tetrahedral elements.

Calay et al. (2002) studied the respiratory flow patterns in a single first-generation bifurcation distal to the trachea and in a multiple-bifurcation model, with their three generations based on the anatomy given by Horsfield et al. (1971). They used four different grid densities comprising, respectively, 31,104, 79,820, 159,872 and 320,980 nodes. Lee and Lee (2002) generated a 3D conduit network model with four generations which conformed closely to Weibel (1963) model in order to study aerosol bolus dispersion. The total number of cells in their 90° out-of-plane model ranged from 40,000 to 60,000. Liu et al. (2003) studied the 3D inspiratory flow in a third-generation asymmetric model from the 5th to the11th branches of Weibel's B model. Kleinstreuer and Zhang (2003) analyzed targeted aerosol drug deposition analysis in a rigid triple-bifurcation tracheobronchial airway model. Their model represents the symmetrically bifurcating generations G3–G6 as in Weibel's lung model with three different hemispherical tumor models placed along the side wall of the G5 airway. Their final mesh comprised about 360,000 cells for the triple-bifurcation configuration. Nowak et al. (2003) demonstrated a four-subunit CFD simulation

*Corresponding author. Tel.: +1 702 443 0215; fax: +1 702 974 1004.
E-mail address: tgemci@yahoo.com (T. Gemci).

0021-9290/$ - see front matter © 2008 Published by Elsevier Ltd.
doi:10.1016/j.jbiomech.2007.12.019

method for the human tracheobronchial tree. They economized on computational effort by segmenting the first 12 generations into four 3.5-generation "tranches" (G0–G3, G3–G6, G6–G9, and G9–G12), without adequately accounting for the fluctuation in boundary conditions between each tranche. Their results indicate dramatic differences in the predicted particle deposition patterns between the two models. The absence of airway curvature and surface irregularities in a Weibel-based model renders the flow fields very different from those in a real human lung (CT-based model). Cebral and Summer (2004) studied the central tracheal and bronchial airways down to four generations by using a virtual bronchoscopy reconstruction method. Airflow patterns resulting from airway stenoses in generations from G0 to G4 were simulated computationally. van Ertbruggen et al. (2005) studied the gas flow and particle deposition in a realistic 3D model of the bronchial tree, extending from the trachea to the segmental bronchi (seventh airway generation for the most distal airways), based on the morphometrical data of Horsfield et al. (1971). Considering symmetric double-bifurcation models, Longest and Vinchurkar (2007b) have recently assessed the effects of upstream transition to turbulence on the flow field and particle deposition in the generations G3–G5 of the respiratory tract. Turbulence was shown experimentally to influence the local deposition of 10-mm-diameter particles, primarily by influencing the initial velocity and particle profiles. Their results underline the importance of correct inlet conditions and the need to consider upstream effects in experimental and computational studies of the respiratory tract. In addition, Longest et al. (2006) compared flow patterns and particle deposition in both normal and childhood asthma-induced constricted models of pulmonary tree generations G3–G5 and G7–G9. Both laminar solutions and the low Reynolds number (LRN) κ–ω turbulence model were employed using a Fluent-6 software package along with their own Fortran and C programs. The authors concluded that airway constriction caused local cellular-level deposition rates to increase by one to two orders of magnitude. Asthma constriction may significantly increase branch-averaged particle deposition with larger increases in local cellular-level deposition, resulting in an aggravated health risk.

More realistic anatomical models have been published by Kitaoka et al. (1999), Tawhai et al. (2000, 2004), Spencer et al. (2001), Tgavalekos et al. (2003), Sera et al. (2003), and Schmidt et al. (2004), using both mathematical algorithms and new experimental imaging techniques. Kitaoka et al. (1999) introduced a 3D model of the human airway tree down to the terminal bronchioles, which by a deterministic algorithm that incorporated duct branching and space division. Tawhai et al. (2000, 2004) developed a 3D tree-growing algorithm specific to a given host geometry derived from magnetic resonance imaging (MRI). Spencer et al. (2001) developed a dynamic surface modeling technique based on data from idealized models to construct 3D computer simulations of tubular pulmonary airway structures within lungs extending from the trachea (G0) to the alveoli (G23). Sera et al. (2003) developed a two-step method to visualize small airways in detail by staining excised rodent pulmonary airways with a radio-opaque solution and then visualizing the tissue with a cone-beam microfocal X-ray CT system. Tgavalekos et al. (2003) advanced the 3D airway tree model of Kitaoka et al. (1999) to predict pulmonary function on the basis of airway structure, particularly when constriction patterns are imposed heterogeneously on the pulmonary tree in specific anatomic locations and compared their model predictions with ventilation images obtained from positron emission tomography (PET) and measurements of dynamic mechanical pulmonary function. The current study includes these upper generations as well as both central and lower tracheobronchial airways within the new 17-generation model.

2. Current 17-generation anatomical model

We have based our present CFD analysis on the best published anatomically explicit human lung model available to date; i.e. the 17-generation anatomical model developed by Schmidt et al. (2004). Fig. 1 represents the anatomy of the human lung of an adult male, free of pathological alterations. Fig. 1a portrays a realistic 3D surface representation of the segmented volume of the bronchial tree. The conduit model reconstructed from an abstracted and adapted topological graph, as shown in Fig. 1b, contains 1453 bronchi up to the 17th Horsfield order. To the authors' knowledge, the computational study described herein represents the first published CFD simulation of the airflow in a digital reference model up to a maximum 17 generations of the total 26 generations of the human tracheobronchial airways with 1453 bronchi. The computer-generated symmetric human lung model of Spencer et al. (2001) for the 23-generation tree lacks the required anatomical detail and accuracy for the current computational investigation and is not as accurate as the Schmidt et al. (2004) anatomical airway model.

The mouth and glottis have not been included in the present 17-generation pulmonary model. It is unlikely that this exclusion will have a direct effect upon the downstream flow as there is a gradual recovery of pressure by the distal end of the trachea (Ma and Lutchen, 2006). The pressure difference, averaged over the luminal cross-section from the proximal to the distal end of the trachea, is insignificant in comparison to the pressure difference between the upper and lower airways as indicated by Ma and Lutchen (2006), and the viscous pressure drop in the trachea was found to be negligible. Thus, the trachea appears to have negligible influence on total lung resistance.

3. CFD simulation

Our characterization of the anatomy of airways must be sufficiently realistic as we intend to extend the present

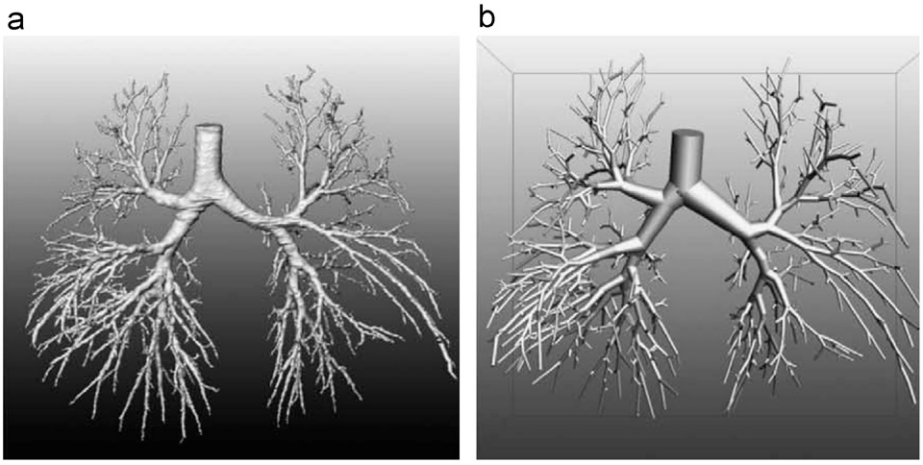

Fig. 1. 3D anterior visualization of bronchial tree models from Schmidt et al. (2004): (a) surface representation of segmented volume data and (b) visualization of a tube model reconstructed from abstracted topological graph data. Reprinted by permission of Elsevier Ltd.

model to design more efficient delivery of inhaled medications and to understand better the health effects of inhaled pollutants. Particle deposition patterns in the branching tracheobronchial network are highly influenced by the detailed branching structures of the human lung, which are important for optimizing aerosol therapy protocols.

In this study, the incompressible airflow in a comprehensive digital reference model was computed using the commercial CFD code (Fluent Inc., 2004). FLUENT® employs a finite-volume method to solve the Navier–Stokes and continuity equations on an arbitrarily shaped flow domain with appropriate boundary conditions and incorporates various two-parameter models (k–ε and k–ω) turbulence models and large eddy simulation (LES). Our computations were performed on two different supercomputing platforms: (1) a RackSaver® cluster at the National Supercomputing Center for Energy and Environment NSCEE at UNLV and (2) a tera-scale machine at the Pittsburgh Supercomputing Center. The steady-state solution of the flow field was assumed to have converged when the residuals reduced to less than 10^{-4}. A typical run time took approximately 50 h on the NSCEE machine.

Computations were performed at 28.3 L/min for a quasi-steady-state volumetric adult inhalation flow rate and as well as at 6, 12, 18, 24, and 30 L/min for the study of static pressure variation.

3.1. Human bronchial tree model and mesh generation

The computational mesh is generated using GAMBIT® software, after transporting into it the abstracted topological graph data from Schmidt et al. (2004). The tube-like surface representation shown in Fig. 1b still retains the exact anatomical asymmetry and branching angles based on a computationally affordable mesh size consisting of 6.744×10^6 unstructured tetrahedral cells as shown in Fig. 2. The mesh generation file is 660 MB and takes 1 h to develop on the tera-scale machine of PSC.

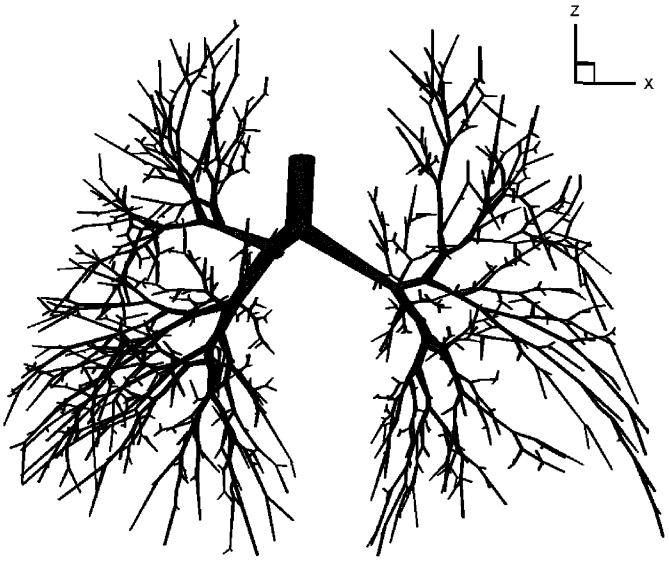

Fig. 2. Anterior view of generated mesh of 17 generations of pulmonary airways (1453 bronchi) with 6.744×10^6 unstructured tetrahedral cells based on abstracted topological graph data from Schmidt et al. (2004). The computational cells cannot be seen in this image.

Longest and Vinchurkar (2007a) applied a grid convergence index (GCI) to four mesh styles of a double-bifurcation model and established grid convergence criteria for both the flow field and particle deposition results using Fluent 6 software. The number of cells needed to resolve fully the geometry of this 17-generation computational model is currently not practical. Due to current hardware limitations, one can only use approximately 6 million control volumes. Full grid convergence will necessarily be left to a future work.

3.2. Numerical methods

The steady-state mass conservation (Eq. (1)) and momentum equations (Eq. (2)) were solved using a

finite-volume method to compute the particle-free fluid flow field. Air was assumed here to be an incompressible, Newtonian fluid with constant density ρ, viscosity μ and fluid static pressure p. The continuity and steady-state Navier–Stokes equations for viscous incompressible Newtonian fluid are given as

$$\frac{\partial u_i}{\partial x_j} = 0 \tag{1}$$

$$\rho u_j \frac{\partial u_i}{\partial x_j} = -\frac{\partial p}{\partial x_i} + \frac{\partial}{\partial x_j}\left(\mu\left(\frac{\partial u_i}{\partial x_j} + \frac{\partial u_j}{\partial x_i}\right) - \rho u'_i u'_j\right) \tag{2}$$

where

$$-\rho u'_i u'_j = \mu_T\left(\frac{\partial u_i}{\partial x_j} + \frac{\partial u_j}{\partial x_i}\right)\frac{2}{3}\rho k \delta_{ij} \tag{3}$$

In order to model the turbulent airflow, we employed a LES model, in which large energy containing eddies are computed directly, while the remaining smaller eddies are modeled using a subgrid-scale (SGS) turbulence model.

3.3. Boundary conditions

The quasi-steady-state inlet velocity is taken here as 2.896 m/s, based on a tracheal inlet area of 162.86 mm^2 and a tracheal diameter of 14.4 mm. A uniform inlet velocity field boundary condition is applied at the tracheal inlet section (G0). The pressure at each outlet (total of 720 outlets) must be known *a priori*, reflecting the effect of the remaining truncated generations G18–G26 at the alveolar level. An alternative approach to setting the flow division ratios would be to use the flow ratio values given by Horsfield et al. (1971). Ma and Lutchen (2006) attempted this, but the pressures computed at the 13 outlets of the G6 large airway model were unacceptably inaccurate, since this is a pressure-driven flow. Accordingly, we recommend the use of mass distributions to determine outflow boundary conditions. The conclusions of Ma and Lutchen (2006) regarding flow versus outlet pressure boundary conditions at the end of G6 do not appear relevant to our model which comprises almost the complete anatomical replica of the pulmonary tree down to the 17th generation level, at which level a constant output $p = 0$ boundary conditions is clearly more appropriate than at the upstream G6 level. From Ma and Lutchen (2006) it appears that turbulence does not have a significant effect on the total input impedance.

We used an inflow boundary condition at G0 and specified pressure outlet boundary conditions at all terminal bronchi exits. The total diameter-dependent mass flow rate at all bronchial exits approximates the inlet value to within 11.2×10^{-6} g/s. No-slip boundary conditions were assumed at the tracheobronchial airway walls. Generation G0 and the first bifurcation were represented by a less dense mesh (1.063×10^6 cells) than for the remaining generations (5.680×10^6 cells) as the flow was more uniform at this upstream location. The computational mesh, with a total of 6.744×10^6 cells, was divided into 1.063×10^6 tetrahedral cells in the G0 zone and into 5.680×10^6 unstructured tetrahedral cells in the remaining zones.

4. Results and discussions

4.1. Tracheobronchial model up to a maximum 17 generations

During inhalation, the flow transitions from laminar to turbulent flow in the larynx and in the tracheal section, and continues into the first main generation. In the conducting zone, containing the trachea, bronchi, bronchioles, and the terminal bronchioles, there is no gas-blood exchange. The downstream increase in cross-sectional area causes a drop in airway pressure and flow rate, such that final air-blood exchange occurs by diffusion at the alveolar level. Our CFD calculations indicate that the static pressure drop is 50 Pa for a volumetric gas flow rate of 28.3 L/min over the complete span as shown in color-coded Fig. 3.

Pressure drop in the bifurcating airways plays an essential role in the respiratory process. Secondary flows in the tracheobronchial airways can be very pronounced. Pedley et al. (1971) and Pedley (1977) determined the static pressure variation to be 60 Pa along Weibel's symmetric bronchial tree, in reasonably good agreement with the experimental measurement by Hyatt and Wilcox (1973) of 75 Pa across the entire respiratory tract. Our comprehensive 3D CFD simulation of the asymmetric bronchial tree model predicted a reasonable static pressure drop of 50 Pa for a steady-state flow rate of 28.3 L/min, corresponding to

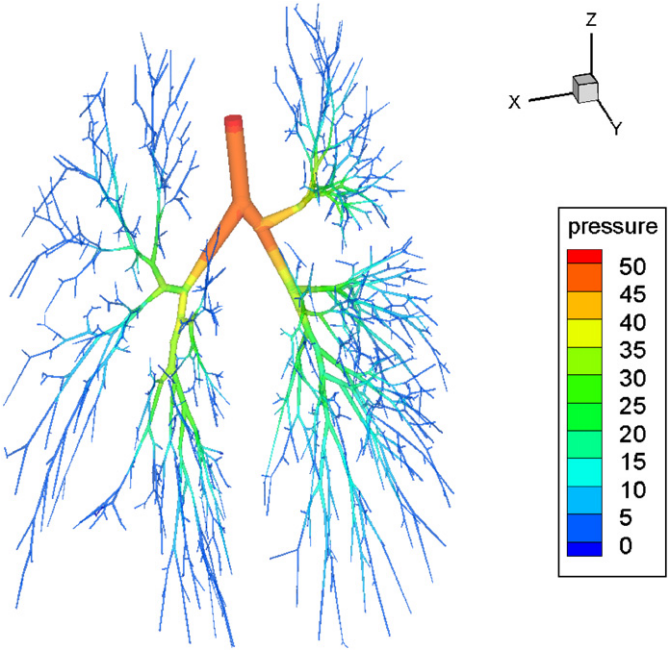

Fig. 3. Pressure distributions across the 17-generation bronchial tree model (posterior view) for a volumetric gas flow rate of $\bar{Q}_g = 500\,\text{cm}^3/\text{s}$ (30 L/min).

normal adult breathing conditions. The viscous pressure drop increases nonlinearly from 6 Pa at 100 cm^3/s to 54 Pa at 500 cm^3/s, as shown in Fig. 4.

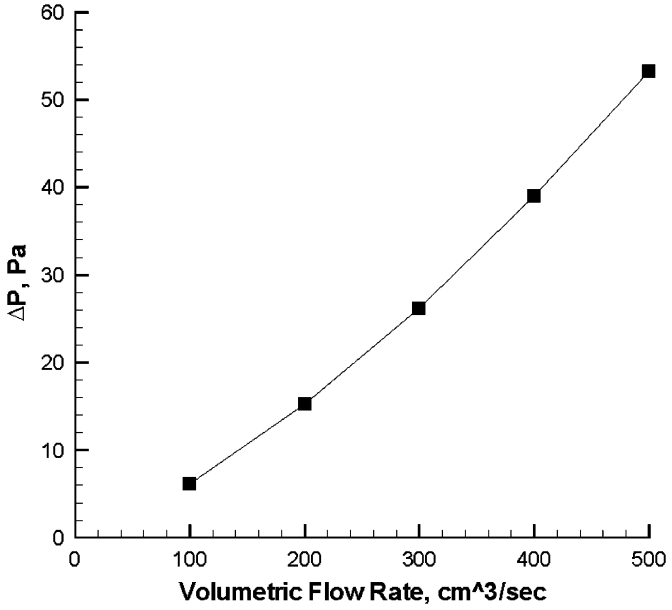

Fig. 4. Pressure drop across the 17-generation bronchial tree model as a function of volumetric gas flow rate from 100 to 500 cm^3/s (6–30 L/min, respectively).

The viscous pressure drop over two selected airway path lines is shown in Fig. 5. The local pressure drops differ because of the anatomical asymmetries between right and left lungs along the two selected path lines. The same trend was observed for a CFD simulation of seven generations (see Fig. 8 in van Ertbruggen et al. (2005) and in the formula for airway pressure drop of Pedley, 1977).

Flow partitioning in the lung is due to anatomical asymmetry of the right and left lungs and influences aerosol deposition. Fig. 6 depicts the percentage change in mass flow rate in the first three generations of the right and left lungs. Generally, the lateral daughter branch attracts much more fluid flow than does the medial branch, as was also observed by Liu et al. (2003).

4.2. *Airflow velocity fields*

Airflows in the upper airways can periodically exhibit the characteristics of laminar, transitional, or fully developed turbulent flow during inhalation due to a succession of conduit cross-sectional area changes occurring between the trachea and the respiratory surfaces of the lungs.

A uniform velocity profile was imposed computationally at the inlet to the trachea with an average value of 2.896 m/s, corresponding to a steady-state inhalatory flow rate of 28.3 L/min and a tracheal diameter of 14.4 mm. At normal breathing rates of 28.3 L/min, the airflow in the larynx and

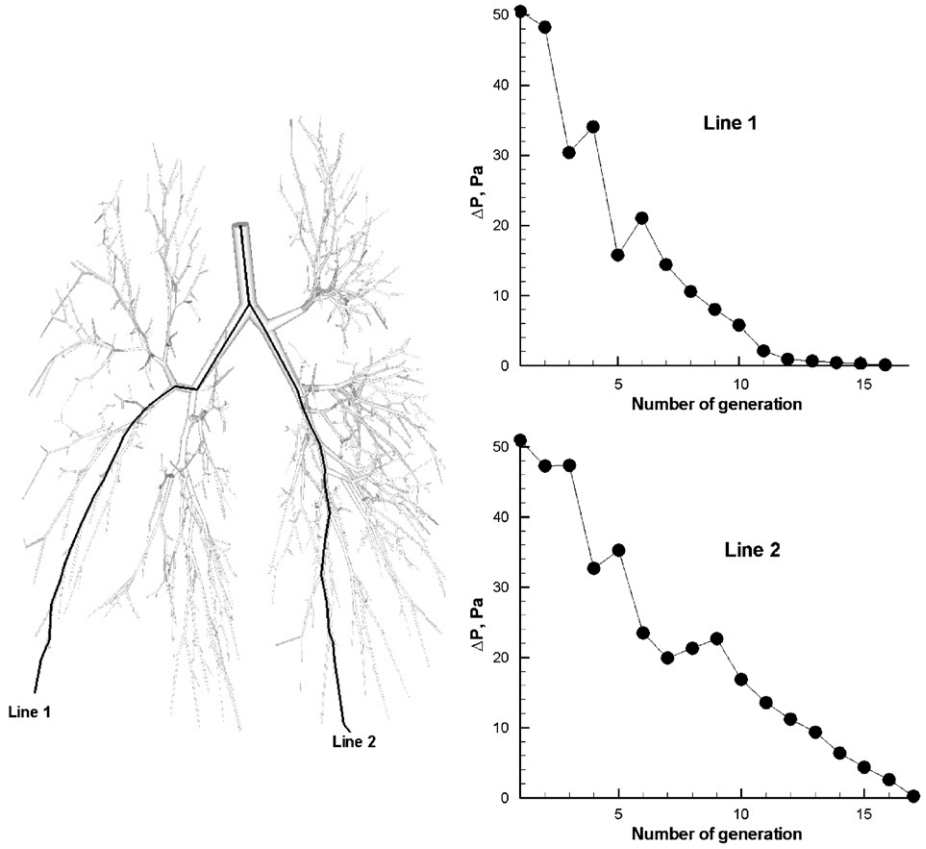

Fig. 5. Variation of the pressure drop along two selected path lines for the flow rate of 28.3 L/min.

in the tracheal section of the upper airways is slightly turbulent. Distal to the first few main upper generations, the airflow quickly transitions to laminar flow. The effects of the turbulent laryngeal jet on the gas flow field extend throughout the length of the larynx, causing recirculatory flows and turbulent eddies even beyond the tracheal bifurcations (Gemci et al., 2002, 2003). Stapleton et al. (2000) and Allen et al. (2004) have shown that the choice of a reasonable turbulence model is critical. For this reason, we performed our airflow simulation with the LES turbulence model, even though it is computationally more expensive than RANS-based turbulence models.

The velocity fields in more anatomically realistic tracheobronchial airway models are more complex than those in the Weibel-based models. Airway curvature and complex anatomical shapes at junctions contribute to those complex flow patterns as noted in Nowak et al. (2003). Figs. 7 and 8 depict the secondary flow patterns in the main left and right bronchi. In previous symmetric and asymmetric Weibel-based tracheobronchial airway models (Pedley et al., 1971; Guan and Martonen, 2000; Calay et al., 2002; Zhang et al., 2002; Liu et al., 2003; Nowak et al., 2003; Shi et al., 2004), the secondary flow in the in-plane cross-section of the bronchus was directed from the center of the inner wall towards the center of the outer wall; it then divided equally into a double vortex, also known as Dean flow. Dean flow was also observed here.

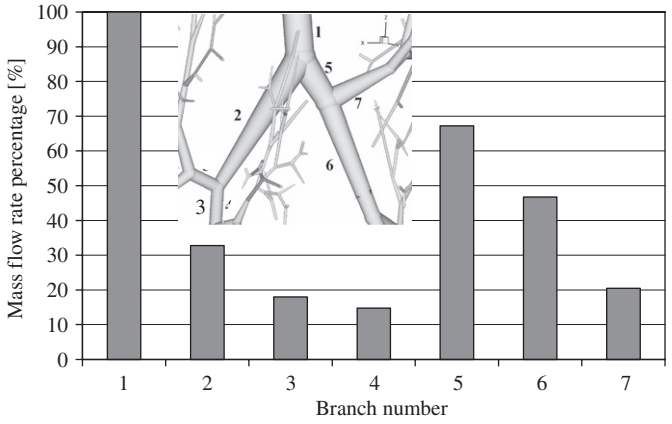

Fig. 6. Percentage variations of the mass flow rate portioning in the first main bifurcation and its distal daughter branches. Total mass flow rate is 0.6125 g/s (corresponding 500 cm^3/s or 30 L/min).

5. Conclusions

CFD evaluations of the quasi-steady incompressible airflow in the human respiratory tract have been presented here with a view to their subsequent extension to the study of the uptake of particulate matter by the tracheobronchial airways in flows varying periodically in time.

We have adapted the anatomical graph data of Schmidt et al. (2004), based on measurements derived from high-resolution computer tomography (HRCT). Assumed pressure drops across successive bifurcations agree reasonably well with earlier published results using more limited anatomical models. Laminar–turbulent flow transitions have been accounted for with a LES model. The computed flow fields also reflect the development of secondary swirling flows resulting from airway curvature.

This digital reference model of the human pulmonary tree is proposed as a first step toward the development of detailed time-varying deposition models with a view to the quantitative design and assessment of therapeutically

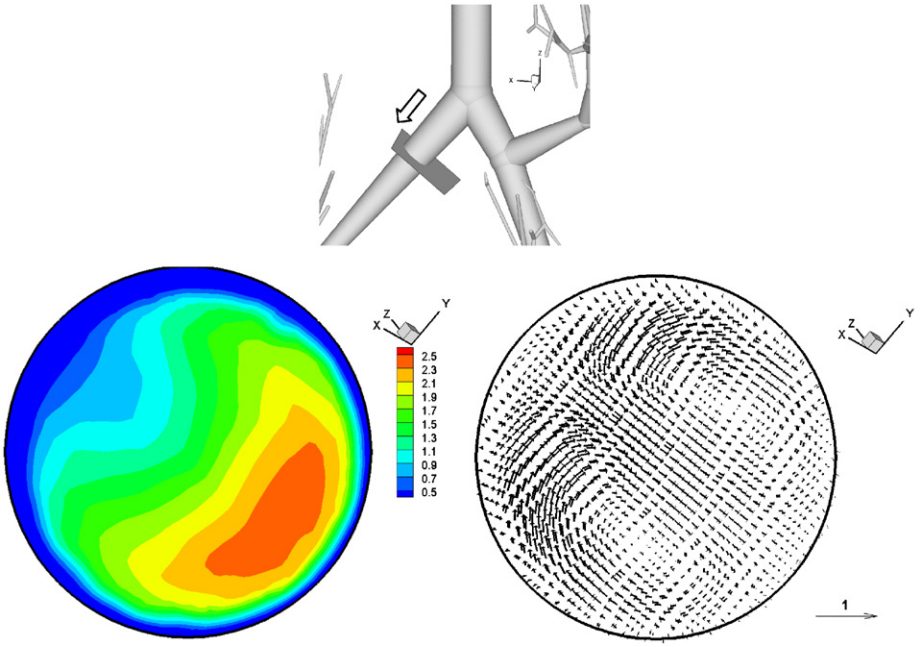

Fig. 7. The velocity vector (right frame) and velocity magnitude (left frame) are shown at an in-plane cross-section at the left main bronchus in the top frame. Pictured here is an oblique plane view of the first left bronchus in a direction perpendicular to the flow.

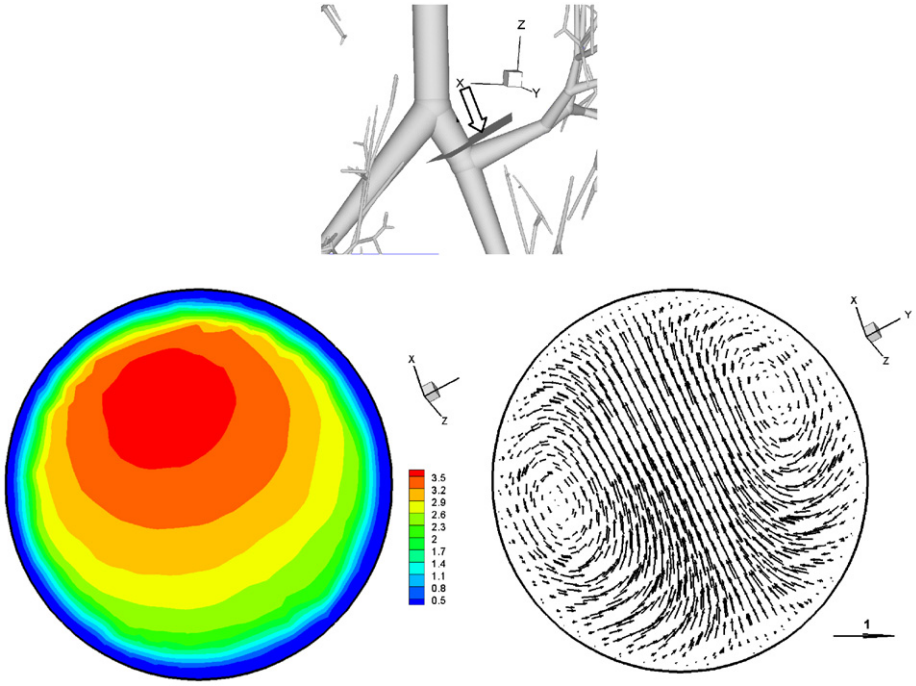

Fig. 8. The velocity vector (right frame) and velocity magnitude (left frame) are shown at an in-plane cross-section at the right main bronchus in the top frame. Pictured here is an oblique plane view of the first right bronchus in a direction perpendicular to the flow.

targeted drug delivery systems via the respiratory tract and to the regional evaluation of the ingestion of particulate pollutants into the respiratory tract.

Conflict of interest

We do not have any conflict of interest.

Acknowledgments

We express our thanks to Dr. Andres Kriete at the Coriell Institute for Medical Research, Camden, NJ for providing us with the abstracted topological graph data. The access to the supercomputers at NSCEE of UNLV and Pittsburgh Supercomputing Center (Grant #CTS010015P) is also gratefully acknowledged.

References

Allen, G.M., Shortall, B.P., Gemci, T., Corcoran, T.E., Chigier, N.A., 2004. Computational simulations of airflow in an in vitro model of the pediatric upper airways. ASME Journal of Biomechanical Engineering 126, 604–613.

Calay, R.K., Kurujareon, J., Holdø, A.E., 2002. Numerical simulation of respiratory flow patterns within the human lung. Respiratory Physiology and Neurobiology 130, 201–221.

Cebral, J.R., Summer, R.M., 2004. Tracheal and central bronchial aerodynamics using virtual bronchoscopy and computational fluid dynamics. IEEE Transactions on Medical Imaging 23 (8), 1021–1023.

Fluent Inc., 2004. Fluent 6.1.18 User's Guide, Lebanon, NH.

Gemci, T., Corcoran, T.E., Chigier, N., 2002. A numerical and experimental study of spray dynamics in a simple throat-model. Aerosol Science and Technology 36 (1), 18–38.

Gemci, T., Shortall, B., Allen, G., Corcoran, T.E., Chigier, N.A., 2003. CFD study of the throat during aerosol drug delivery using heliox and air. Journal of Aerosol Science 34, 1175–1192.

Guan, X., Martonen, T.B., 2000. Flow transition in bends and applications to airways. Journal of Aerosol Science 31 (7), 833–847.

Horsfield, K., Dart, G., Olson, D.E., Filley, G.F., Cumming, G., 1971. Models of the human bronchial tree. Journal of Applied Physiology 31, 207–217.

Hyatt, R.E., Wilcox, R.E., 1973. The pressure-flow relationship of the intrathoracic airways in man. Journal of Clinical Investigation 42, 29–39.

Kitaoka, H., Takaki, R., Suki, B., 1999. A three-dimensional model of the human airway tree. Journal Applied Physiology 87 (6), 2207–2217.

Kleinstreuer, C., Zhang, Z., 2003. Targeted drug aerosol deposition analysis for a four-generation pulmonary airway model with hemispherical tumors. ASME Journal of Biomechanical Engineering 125, 197–206.

Kriete, A., Schmidt, A.H., Zidowitz, S., Haworth, D.C., Kunz, R.F., 2004. Simulations at a newly derived reference model of the human lung. Proceedings of SPIE 5318, 163–169.

Lee, D.Y., Lee, J.W., 2002. Dispersion of aerosol bolus during one respiration cycle in a model of pulmonary airways. Journal of Aerosol Science 33, 1219–1234.

Liu, Y., So, R.M.C., Zhang, C.H., 2003. Modeling the bifurcating flow in an asymmetric human pulmonary airway. Journal of Biomechanics 36, 951–959.

Longest, P.W., Vinchurkar, S., 2007a. Effects of mesh style and grid convergence on particle deposition in bifurcating airway models with comparisons to experimental data. Medical Engineering and Physics 29 (3), 350–366.

Longest, P.W., Vinchurkar, S., 2007b. Validating CFD predictions of respiratory aerosol deposition: effects of upstream transition and turbulence. Journal of Biomechanics 40, 305–316.

Longest, P.W., Vinchurkar, S., Martonen, T.B., 2006. Transport and deposition of respiratory aerosols in models of childhood asthma. Journal of Aerosol Science 37, 1234–1257.

Ma, B., Lutchen, K.R., 2006. An anatomically based hybrid computational model of the human lung and its application to low frequency oscillatory mechanics. Annals of Biomedical Engineering 34 (11), 1691–1704.

Nowak, N., Kakade, P.P., Annapragada, A.V., 2003. Computational fluid dynamics simulation of airflow and aerosol deposition in human lungs. Annals of Biomedical Engineering 31, 374–390.

Pedley, T.J., 1977. Pulmonary fluid dynamics. Annual Review of Fluid Mechanics 9, 229–274.

Pedley, T.J., Schroter, R.C., Sudlow, M.F., 1971. Flow and pressure drop in systems of repeatedly branching tubes. Journal of Fluid Mechanics 46, 365–383.

Schmidt, A., Zidowitz, S., Kriete, A., Denhard, T., Krass, S., Peitgen, H.-O., 2004. A digital reference model of the human bronchial tree. Computerized Medical Imaging and Graphics 28, 203–211.

Sera, T., Fujioka, H., Yokota, H., Makinouchi, A., Himeno, R., Schroter, R.C., Tanishita, K., 2003. Three-dimensional visualization and morphometry of small airways from microfocal X-ray computed tomography. Journal of Biomechanics 36, 1587–1594.

Shi, H., Kleinstreuer, C., Zhang, Z., 2004. Nanoparticle transport and deposition in bifurcating tubes with different inlet conditions. Physics of Fluids 16 (7), 2199–2213.

Snyder, B., Dantzker, D.R., Jaeger, M.J., 1981. Flow partitioning in symmetric cascades of branches. Journal of Applied Physiology 51 (3), 506–598.

Spencer, R.M., Schroeter, J.D., Martonen, T.B., 2001. Computer simulations of pulmonary airway structures using data-driven surface modeling techniques. Computers in Biology and Medicine 31, 499–511.

Stapleton, K.W., Guentsch, E., Hoskinson, M.K., Finlay, W.H., 2000. On the suitability of *k*–epsilon modeling for aerosol deposition in the mouth and throat: a comparison with experiment. Journal of Aerosol Science 31, 739–749.

Tawhai, M.H., Pullan, A.J., Hunter, P.J., 2000. Generation of an anatomically based three-dimensional model of the conducting airways. Annals of Biomedical Engineering 28, 793–802.

Tawhai, M.H., Hunter, P., Tschirren, J., Reinhardt, J., McLennan, G., Hoffman, E.A., 2004. CT-based geometry analysis and finite element models of the human and ovine bronchial tree. Journal Applied Physiology 97 (6), 2310–2321.

Tgavalekos, N.T., Venegas, J.G., Suki, B., Lutchen, K.R., 2003. Relation between structure, function, and imaging in a three-dimensional model of the lung. Annals of Biomedical Engineering 31, 363–373.

van Ertbruggen, C., Hirsch, C., Paiva, M., 2005. Anatomically based three-dimensional model of airways to simulate flow and particle transport using computational fluid dynamics. Journal of Applied Physiology 98 (3), 970–980.

Zhang, Z., Kleinstreuer, C., 2004. Airflow structures and nano-particle deposition in a human upper airway model. Journal of Computational Physics 198, 178–210.

Zhang, Z., Kleinstreuer, C., Kim, C.S., 2002. Cyclic micron-size particle inhalation and deposition in a triple bifurcation lung airway model. Journal of Aerosol Science 33, 257–281.

Zhao, Y., Lieber, B.B., 1994. Steady inspiratory flow in a model symmetric bifurcation. ASME Journal of Biomechanical Engineering 116, 488–496.

Weibel, E.R., 1963. Morphometry of the Human Lung. Springer, Berlin.